diabetes®
American Diabetes Association®

Combined Weight Loss and Exercise Training Alters Skeletal Muscle Subcellular Lipid Localization and Intermuscular Adipose Tissue Cellular Composition

Karin Zemski Berry, Amanda Garfield, Katie L. Whytock, Emily Macias, Simona Zarini, Purevsuren Jambal, Tyler Stepaniak, Sophia Bowen, Leigh Perreault, Chris Johnson, Darcy Kahn, Anna Kerege, Ian J. Tamburini, Christy M. Nguyen, Carlos H. Viesi, Marcus Seldin, Yifei Sun, Martin Walsh, Lauren M. Sparks, and Bryan C. Bergman

Diabetes 2025;74(12):1–15 | https://doi.org/10.2337/db25-0492

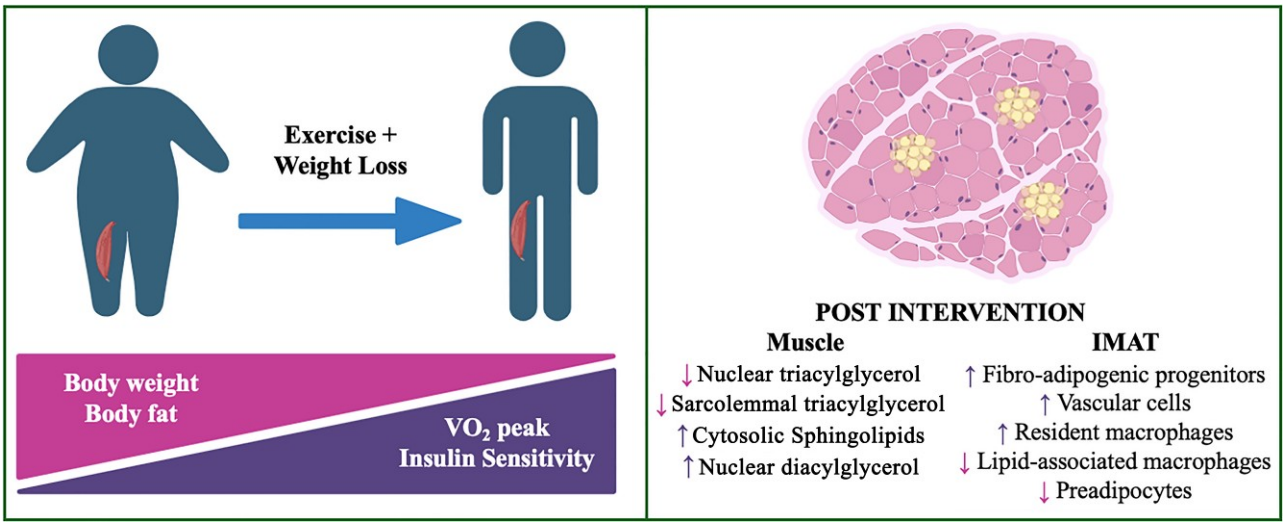

Combined Weight Loss and Exercise Training Alters Skeletal Muscle Subcellular Lipid Localization and Intermuscular Adipose Tissue Cellular Composition

Karin Zemski Berry,[1] Amanda Garfield,[1] Katie L. Whytock,[2] Emily Macias,[1] Simona Zarini,[1] Purevsuren Jambal,[1] Tyler Stepaniak,[1] Sophia Bowen,[1] Leigh Perreault,[1] Chris Johnson,[1] Darcy Kahn,[1] Anna Kerege,[1] Ian J. Tamburini,[3] Christy M. Nguyen,[3] Carlos H. Viesi,[3] Marcus Seldin,[3] Yifei Sun,[4] Martin Walsh,[4] Lauren M. Sparks,[2] and Bryan C. Bergman[1]

https://doi.org/10.2337/db25-0492

Subcellular lipid accumulation and intermuscular adipose tissue (IMAT) accumulation are associated with insulin resistance, but the impact of combined weight loss and exercise training on localization of lipids and IMAT cellular composition is not known. Twenty-one adults with obesity (18 female and 3 male; 46 ± 2 years; 35.0 ± 0.9 kg/m^2) completed a 3-month supervised weight loss and exercise training intervention. Insulin sensitivity was measured using a hyperinsulinemic-euglycemic clamp, and basal and insulin-stimulated vastus lateralis biopsies were collected pre- and postintervention. After the intervention, body weight and body fat decreased (11 ± 1% and 9 ± 1%, respectively), while VO_2 peak and insulin sensitivity increased (14 ± 3% and 68 ± 14%, respectively). Lipidomics revealed reduced sarcolemmal and nuclear triglycerides, with unchanged whole-muscle triglycerides. Whole-muscle diacylglycerols increased because of increased nuclear 1,2-diacylglycerols without PKCε, PKCθ, or PKCδ activation. Whole-muscle sphingolipid levels increased because of cytosolic accumulation. Single-nuclei RNA sequencing showed altered IMAT cellular composition, including increased fibro-adipogenic progenitors, vascular cells, and macrophages, and decreased preadipocytes. Bulk muscle RNA sequencing indicated upregulation of genes related to muscle remodeling and cellular respiration, and there were changes in the relationship between nuclear diacylglycerols and gene expression postintervention. These findings dissociate improvements in insulin sensitivity from total muscle diacylglycerol and sphingolipid levels and highlight roles for subcellular lipid redistribution and IMAT remodeling in insulin sensitization.

ARTICLE HIGHLIGHTS

- Evaluation of subcellular fractionated muscle revealed decreases in sarcolemmal and nuclear triglycerides and increases in nuclear diacylglycerols and cytosolic sphingolipids postintervention.
- Weight loss revealed alteration in the cellular composition of intermuscular adipose tissue and upregulation of genes related to muscle remodeling and cellular respiration.
- These findings dissociate improvements in insulin sensitivity from total muscle 1,2-diacylglycerol and sphingolipid levels and highlight roles of intermuscular adipose tissue remodeling for enhanced insulin sensitivity.

Muscle lipid accumulation is linked with lower muscle insulin sensitivity in humans, except in athletes who have muscle lipid accumulation yet remain insulin-sensitive, a phenomenon known as the Athlete's paradox (1). Muscle contains numerous classes of lipids with many molecular species, making the interpretation of muscle lipid accumulation complex. Evidence suggests that bioactive lipids

[1]School of Medicine, University of Colorado Anschutz Medical Campus, Aurora, CO
[2]Translational Research Institute, Orlando, FL
[3]School of Medicine, University of California, Irvine, CA
[4]Icahn School of Medicine at Mount Sinai, New York, NY
Corresponding author: Bryan C. Bergman, Bryan.Bergman@cuanschutz.edu

Received 22 May 2025 and accepted 24 August 2025

This article contains supplementary material online at https://doi.org/10.2337/figshare.29980063.

Clinical trial reg. no. NCT02043405, clinicaltrials.gov

such as 1,2-diacylglycerol (1,2-DAG) and sphingolipids play an important role in decreasing insulin sensitivity in muscle, with some studies suggesting only specific species of 1,2-DAG and sphingolipids play a deleterious role (2–4). However, the total content and specific species of bioactive lipids do not always account for differences in insulin sensitivity between individuals or in response to interventions (5–7). Emerging evidence suggests that other factors, such as subcellular localization, may play an important role. Reports from several groups, including our laboratory, suggest that the intracellular localization of skeletal muscle lipids influences how specific lipid species affect insulin sensitivity (8–10). Overall, the literature supports the idea that intracellular lipid content, composition, and subcellular localization impact insulin sensitivity in muscle. Insulin-sensitizing interventions are needed to clarify the role of subcellular lipid species and their distribution in altering insulin sensitivity.

Beyond intracellular lipids, the content of adipose tissue laced between and within skeletal muscles, called intermuscular adipose tissue (IMAT), directly relates to insulin resistance associated with sex, age, and race and ethnicity (11–13). The IMAT secretome decreases insulin sensitivity when administered to myotubes in vitro (14), which may be due to the inflammatory secretory profile of this unique adipose tissue depot (15). We recently published a single-nuclei RNA sequencing (snRNA-seq) analysis of IMAT that revealed a diverse array of cell types in IMAT, including immune cells (16) that impact inflammatory cytokine secretion. However, it is not known whether the IMAT cellular composition is fixed or whether insulin-sensitizing lifestyle interventions can alter the proportion of cell types in this depot.

The current study was designed to evaluate alterations in bioactive lipid localization and IMAT cellular composition following a combined weight loss and exercise training intervention. We aimed to test the hypothesis that decreased sarcolemmal 1,2-DAG and ceramide are required for insulin sensitization in humans, and to evaluate whether the IMAT cellular composition is malleable.

RESEARCH DESIGN AND METHODS

Participants

Twenty-one individuals with class I or II obesity, with and without prediabetes or newly diagnosed type 2 diabetes, were recruited for this study. Participants gave written informed consent and were excluded if they had a BMI <30 or >40 kg/m^2; had fasting triglycerides >150 mg/dL; or had liver, kidney, thyroid, or lung disease. The age range of participants was 32–60 years old. Newly diagnosed individuals with type 2 diabetes were individuals that were known to have prediabetes but had fasting and 2-h post–oral glucose tolerance test glucose concentrations consistent with type 2 diabetes during preliminary testing. All individuals were sedentary and engaged in planned physical activity <2 h/week. Participants were weight stable in the 6 months prior to the study. This study was approved by the Colorado Multiple Institution Review Board at the University of Colorado Denver.

Overall Study Design

Participants were recruited into a 12-week combined weight loss and exercise training intervention. After initial preliminary testing, food was provided for 1 week before completing a hyperinsulinemic/euglycemic clamp study. Participants spent the night at the research center and, the next morning, underwent a muscle biopsy followed by a standard 3-h insulin clamp with another muscle biopsy 1 h into the insulin infusion. Participants then completed a supervised 12-week combined weight loss and exercise training intervention. After 2 weeks of weight stabilization, all of the preintervention testing was repeated.

Preliminary Testing

Following a 12-h overnight fast, participants reported to the Clinical Translational Research Center for screening procedures, where they were given a health and physical examination, fasting blood draw, standard 75-g oral glucose tolerance test, and DEXA analysis (Lunar DPX-IQ; Lunar Corporation, Madison, WI).

Exercise and Dietary Control

Participants were asked to refrain from planned physical activity for 48 h before the insulin clamp. Food was provided for 7 days prior to the insulin clamp before and after the intervention. Energy requirement was estimated based on DEXA-determined fat-free mass (FFM) according to the previously published equation (daily energy intake = $1.4 \times [372 + (23.9 \times \text{FFM})]$) with the macronutrient intake at 55% carbohydrate, 15% protein, and 30% fat (17). After the first insulin clamp, participants began the combined weight loss and exercise training intervention as described below. When appropriate based on menopausal status, women were tested during the midfollicular phase of the menstrual cycle to control for potential effects on insulin sensitivity.

Hyperinsulinemic-Euglycemic Clamp and Skeletal Muscle Biopsy

After a 12-h supervised overnight fast, a percutaneous vastus lateralis muscle biopsy and hyperinsulinemic-euglycemic clamp with [6,6-$^2H_2$]glucose infusion (Cambridge Isotope Laboratories, Tewksbury, MA) was performed as previously described (8). Muscle was immediately flash frozen in liquid nitrogen. Muscle biopsies were later dissected on ice using a dissection scope at 30× to isolate IMAT from muscle as previously described (18). Contamination of IMAT with small pieces of muscle is expected, and therefore changes in myonuclei gene expression were not evaluated in subsequent snRNA-seq analysis. One hour into the insulin clamp, another muscle biopsy was taken from

the contralateral leg using identical procedures to measure insulin-stimulated insulin signaling.

Weight Loss and Exercise Training Intervention

Volunteers were provided a low-calorie diet consisting of a meal replacement product (HealthOne; Nutrition Technology Inc., Carmel, CA). Participants were asked to consume 2 teaspoons (10 g) per day of vegetable oil, provided powdered HealthOne formula, and instructed to consume five portions per day providing 890 kcal/d, 75 g protein, 15 g fat, and 110 g of carbohydrate, and 100% of the dietary reference intake of all vitamins, minerals, and micronutrients. Participants were allowed to consume noncaloric beverages, but no other food intake was allowed. Participants were seen weekly for sessions with a registered dietitian for nutritional counseling.

Participants also underwent four sessions per week of supervised endurance exercise training by the Nutrition Obesity Research Center energy balance core. Each session lasted 60 min and included a short warm-up, 40 to 50 min of endurance exercise, and a cooldown. The exercise program consisted primarily of brisk walking or jogging supplemented with rowing, stepping, or elliptical exercise. These exercises were chosen to ensure feasibility and comfort for participants. There is variable recruitment of the vastus lateralis during these exercises; for example, there is less recruitment during walking and jogging compared with cycling (19). As a result, variability on the modality of training may have impacted the training adaptations observed from the vastus lateralis biopsy. Individualized exercise prescriptions considered the fitness level of the participant, preferences with regard to type of exercise, and orthopedic limitations. The initial exercise prescription was 30 min at 65% of maximal heart rate (HR), based on the highest HR attained during the baseline maximal exercise test, which was repeated after 6 weeks of training. During the first 2–3 weeks of training, exercise duration and intensity was gradually increased to 45 min at 80% to 85% of maximal HR. The exercise intensity was updated every 2 weeks and was carefully geared to the participant's exercise capacity.

Weight Stability

After the intervention, participants transitioned to a supervised 2-week weight maintenance diet consisting of three servings of meal replacement per day along with one meal of typical foods to stabilize weight. Volunteers continued to exercise during the weight stabilization period and were tested 48 h after the last exercise bout.

Postintervention Testing

After completing the weight stability period of the protocol, individuals repeated the DEXA and VO_2max tests, as well as the 7-day dietary control, prior to repeating the insulin clamp visit.

Skeletal Muscle Fractionation

Muscle biopsies (45–65 mg wet weight) were homogenized on ice using a Teflon-glass homogenizer in fractionation buffer (250 mmol/L sucrose; 5 mmol/L $MgCl_2$; 1 mmol/L EDTA; 20 mmol/L Tris-HCl; 40 mmol/L KCl; pH 7.4) and centrifuged at 100,000*g* for 1 h, and pellets were resuspended in fractionation buffer with DNAse (6.25 μg/mL) as previously described (8). Samples were rehomogenized, layered onto an Optiprep gradient (12–30%), and centrifuged at 60,000*g* for 3 h at 4°C. Sarcolemmal, cytosolic, mitochondrial, and nuclear fractions were collected and analyzed for protein content.

Lipidomics Analysis

Whole-muscle samples (10–15 mg) were homogenized using a bead mill homogenizer for 2 min at 25 Hz, internal standard cocktail was added, and lipid was extracted with 3 mL methyl tert-butyl ether. The cytosolic, sarcolemmal, mitochondrial, and nuclear compartments were extracted similarly without homogenization. Triglycerides, DAGs, sphingolipids, and acylcarnitines were analyzed following previously established methods (20).

snRNA-seq Analysis

Nuclei were extracted from 100–125 mg of pooled pre-IMAT (n = 8) and pooled post-IMAT (n = 5) samples using a previously established protocol (21). Full-length snRNA-seq libraries were generated with the iCELL8 system (Takara Bio) (22). Libraries were sequenced to 250 million reads, yielding ∼150,000 barcoded reads and ∼9,000 genes per nucleus (22). Demultiplexing, mapping, alignment, and counting of the snRNA-seq libraries was performed used the CogentAP Analysis Pipeline (Takara Bio) and GRCh38 as a reference genome. Nuclei were initially filtered if they had <500 genes, >20,000 genes, <10,000 counts, or >10% mitochondrial reads or if cell complexity was <0.75. Genes with low expression (average count less than 0.1) were filtered prior to clustering analyses. Data were normalized in Seurat (V4.4.0) with SCTransform. Data were adjusted for ambient RNA with decontx (23) with cell cluster labels used as the Z parameter before batch integration with harmony (24). Differential gene expression analysis between pre-IMAT and post-IMAT samples was performed using a Wilcoxon rank sum test with Seurat's "FindMarkers" function with a false discovery rate cutoff of <0.05, $\log_2$ fold change >0.1 or less than −0.1 and expressed in >10% of nuclei in that cluster. Enrichment analyses on differentially expressed genes was conducted with TMsig using GeneOntology:Biological Pathways.

Bulk RNA-seq Analysis

Whole muscle (∼15 mg) was pulverized at the temperature of liquid nitrogen, homogenized in Trizol (Invitrogen, Carlsbad, CA), RNA isolated using the RNAeasy Isolation Kit (Qiagen, Hilden, Germany), and then tested for concentration and quality, with samples where the RNA integrity number was >7.0 used in downstream applications. Libraries

were prepared using Lexogen 3′ QuantSeq kits with dual index adapters. A total of 200–1,000 ng of RNA was used for library preparation. Individual libraries were pooled and sequenced using a NovaSeq 6000 (Novagene) following in-house established protocols. Raw RNA-seq reads were inspected for quality using FastQC v0.11.9 (Barbraham Institute, Barbraham, U.K.). Gene expression was quantified using kallisto and aligned to the current human transcriptome build (GRCh38). Lowly expressed genes (less than a sum of 20 transcripts per million across all samples) were removed. Samples were analyzed for differential expression using DeSeq2 v1.28.0.

Western Blotting

Protein expression and phosphorylation were measured using Western blots as previously described by our laboratory (8). Details of the primary and secondary antibodies used for western blots are listed in Supplementary Table 1. Signal values of the protein bands were normalized to the corresponding total or pan values, or β-actin.

PKC Activation

PKC activity was estimated using membrane-to-cytosol ratio of PKC isoforms as previously described (25). Details of the primary and secondary antibodies used for Jess are listed in Supplementary Table 1.

Plasma Glucose Enrichment Analysis

Glucose isotopic enrichment was measured using gas chromatography–mass spectrometry (Thermo ISQ) as previously described (26).

Substrate and Hormone Analyses

Standard enzymatic assays were used to measure glucose (Olympus AU400e Chemistry Analyzer; Olympus America Inc., Center Valley, PA), glycerol (r-Biopharm, Darmstadt, Germany), and free fatty acids (FFA) (NEFA Kit; FUJIFILM Wako Chemicals, Wako, TX). Plasma insulin and glucagon were measured using a radioimmunoassay (Diagnostic Systems Laboratories, Inc., Webster, TX).

Statistical Analysis

Data are presented as mean ± SEM. Differences in normally distributed data between groups were analyzed using a one-way ANOVA (SPSS, Chicago, IL). Significant differences in individual lipid species for each type of lipid within a compartment before and after the intervention were adjusted for multiple comparisons using the Holm-Sidak method. Adjusted *P* values are presented. Significant relationships between muscle lipids were determined using Pearson correlation coefficient and were adjusted for multiple comparisons using the Benjamini-Hochberg procedure. A *P* value of <0.05 was considered significant. Because this cohort was mostly women, sex was not considered as a factor in the statistical analysis of this data.

Data and Resource Availability

The data sets generated in this study are available upon request from the corresponding author. No applicable resources were generated during the study.

RESULTS

Demographic data for those completing the intervention are shown in Table 1. Participants included 3 men and 18 women with an average age of 46 years. After the weight loss by caloric restriction and exercise training intervention, the cohort significantly decreased body weight (kg) by 11% (Cohen's d = −2.4, mean of differences = −10.52, 95% CI [−12.5, −8.5]), increased in VO_2peak (L/min) by 13% (Cohen's d = 1.09, mean of differences = 0.30, 95% CI [0.17, 0.41]) and insulin sensitivity (mg/μU/kg/min) by 68% (Cohen's d = 0.96, mean of differences = 0.02996, 95% CI [0.0154, 0.044]). Percent body fat decreased by 8%, and FFM decreased by 6%, along with decreases in fasting insulin, glucagon, FFA, glycerol, and TNFα (P < 0.05). Participants maintained body weight during the 1-week dietary control before and after the intervention, with an average change in body weight of −0.9 ± 0.2% before and −0.6 ± 0.5% after the intervention. We achieved steady-state conditions during the insulin clamp (Supplementary Fig. 1).

Intramuscular Lipids

Our muscle fractionation protocol was successful in enriching protein markers of sarcolemmal (Na/K ATPase), mitochondrial (voltage-dependent anion channels), nuclear (lamin A–C), and cytosolic fractions (GAPDH) (Supplementary Fig. 2). We achieved 85% enrichment of sarcolemmal fraction, 91% for the mitochondrial fraction, 87% for the nuclear fraction, and 92% of the cytosolic fraction. Perilipin 2 is lipid droplet protein to show that lipid droplets are collected in the cytosolic fraction.

Triglycerides

Significant changes in whole-muscle total triglyceride concentration after the intervention were not observed (Fig. 1*A*). Significant decreases in both sarcolemmal (P = 0.04) (Fig. 1*B*) and nuclear total triacylglycerol (TAG) content (P = 0.04) (Fig. 1*D*) were observed without changes in mitochondrial or cytosolic total TAG (Fig. 1*C* and 1*E*). Species-level detail for sarcolemmal and nuclear triglyceride revealed greater changes in shorter-chain triglycerides compared with longer-chain species in both compartments (Supplementary Fig. 3).

DAG

Whole-muscle concentration of DAGs revealed significant increases in 1,2-DAG (P = 0.01) and total DAG (1,2- + 1,3-DAG, P = 0.008) after the intervention (Fig. 2*A*). However, the increase was confined to 1,2-DAG in the nuclear compartment (P = 0.003), with no significant changes in

Table 1—Subject demographics

	Preintervention	Postintervention
Sex (M/F)	(3/18)	
Age (years)	46.0 ± 1.9	
BMI (kg/m^2)	35 ± 0.9	31.4 ± 0.9*
Weight (kg)	98.5 ± 2.4	87.9 ± 2.4*
Percent fat	41.4 ± 1.3	38.1 ± 1.5*
FFM (kg)	56.9 ± 1.5	53.4 ± 1.4*
VO_2peak (L/min)	2.25 ± 0.1	2.55 ± 0.12*
Insulin sensitivity (clamp glucose Rd normalized to insulin [mg/μU/kg/min])	0.0478 ± 0.004	0.0789 ± 0.008*
Fasting glucose (mg/dL)	101.1 ± 6.6	91.9 ± 2.3
Fasting insulin (μU/mL)	15.1 ± 1.2	10.6 ± 1.1*
Fasting glucagon (pg/mL)	79.3 ± 3.6	70 ± 3.3*
Fasting FFA (μmol/L)	584 ± 26	508 ± 19*
Fasting glycerol (μmol/L)	107.3 ± 6.3	91.7 ± 4.3*
Fasting IL-6 (pg/mL)	1.69 ± 0.15	1.59 ± 0.18
Fasting TNFα (pg/mL)	0.90 ± 0.15	0.68 ± 0.14*

Values are means ± SEM. *Significantly different from preintervention, $P < 0.05$. Rd = rate of disposal.

1,3-DAG (Fig. 2*B–E*). Nuclear unsaturated 1,2-DAG species increased, including C16:0/18:2 ($P = 0.04$), C16:0/20:4 ($P = 0.002$), C18:0/18:1 ($P = 0.01$), and C18:0/18:2 ($P = 0.01$) (Supplementary Fig. 4).

Sphingolipids

Whole-muscle concentrations of sphingosine ($P = 0.009$), total ceramides ($P = 0.007$), and sphingomyelin ($P = 0.0001$) increased after the intervention (Fig. 3*A*). There were no changes in the subcellular distribution of total sphingolipids in the sarcolemmal and mitochondrial compartments (Fig. 3*B* and 3*C*). Increased whole-muscle concentration was due to increases in the nuclear and cytosolic compartments (Fig. 3*D* and 3*E*). We found increased nuclear sphingosine ($P = 0.003$), along with increased concentration of all sphingolipids in the cytosolic compartment (sphingosine, $P = 0.0001$; ceramide, $P = 0.0002$; dihydroceramide, $P = 0.005$; glucosylceramide, $P = 0.003$; lactosylceramide, $P < 0.0001$; sphingomyelin, $P = 0.0002$) (Fig. 3). Significant changes in individual cytosolic sphingolipid species are shown in Supplementary Fig. 5. We found significant correlations between C16:0 and C18:0 species of sphingomyelin and ceramide in the sarcolemma preintervention (C16:0 $R^2 = 0.78$, $P < 0.001$; C18:0 $R^2 = 0.92$, $P < 0.001$) and postintervention (C16:0 $R^2 = 0.87$, $P < 0.001$; C18:0 $R^2 = 0.84$, $P < 0.001$), with stronger relationships than observed for dihydroceramide and ceramide for the same species preintervention (C16:0 $R^2 = 0.66$, $P < 0.001$; C18:0 $R^2 = 0.11$, $P = 0.16$) and postintervention (C16:0 $R^2 = 0.34$, $P = 0.007$; C18:0 $R^2 = 0.39$, $P = 0.004$) (Supplementary Fig. 6). We found no significant differences in the sarcolemmal ratio of sphingomyelin and ceramide, reflecting sphingomyelinase activity (27), before or after the intervention (preintervention: 29.2 ± 1.6; postintervention: 27.6 ± 1.6).

Acylcarnitines

Whole-muscle acylcarnitine concentration increased after the intervention ($P = 0.0005$) (Fig. 4*A*), with significant increases explained by changes only in the nuclear compartment ($P = 0.03$) (Fig. 4*B–E*). Only nuclear 14:0 acylcarnitine species increased after the intervention (Supplementary Fig. 7).

IMAT Cell Composition

snRNA-seq of IMAT revealed eight cell populations including fibro-adipogenic progenitor cell populations (FAPs), two populations of preadipocytes, adipocytes, vascular and immune cells, and the presence of myonuclei (Fig. 5*A*) that were annotated with known marker genes (Fig. 5*B*). Cell composition was compared without myonuclei, as these nuclei are considered an artifact in IMAT processing. An increased proportion of FAPs (+9.94%), vascular cells (+12.5%), and immune cells (+4.45%) and a decrease in a population of Pre_Ad_2 (−25.5%) was observed after the intervention (Fig. 5*C*). Differential gene expression analyses revealed Pre_Ad_2 were enriched in genes related to γ-aminobutyric acid signaling (Supplementary Table 2). We found the most overlap with markers of resident macrophages rather than lipid-associated macrophages (Fig. 5*D*), suggesting remodeling of adipose tissue rather than proinflammatory state (28).

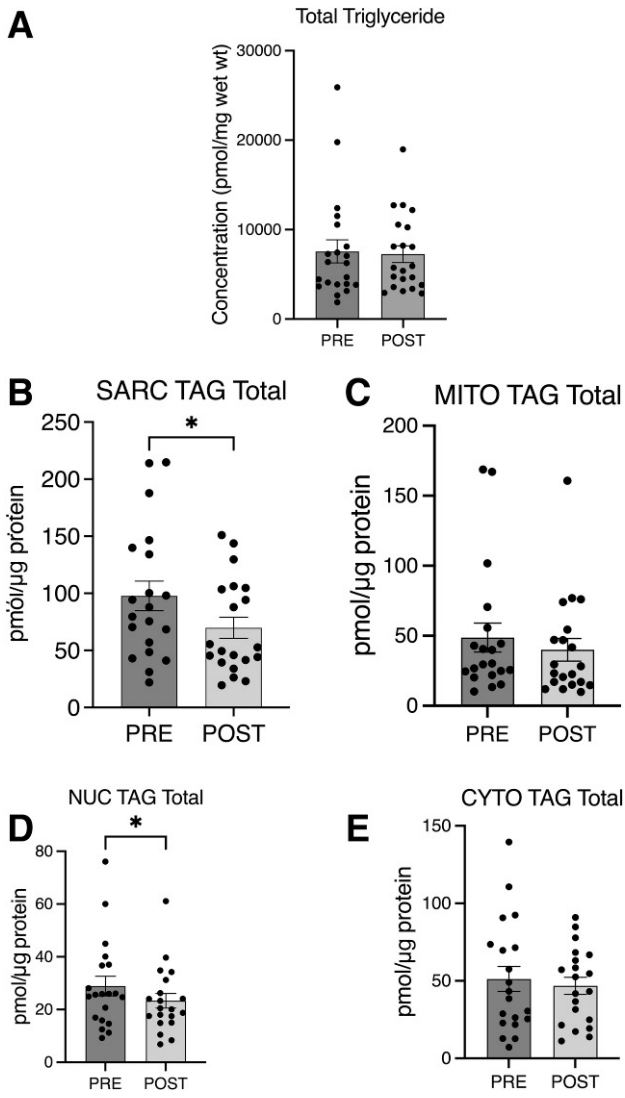

Figure 1—Whole-muscle triacylglycerol (TAG) concentration before and after the intervention (*A*). TAG concentrations are shown for sarcolemmal (*B*), mitochondrial (*C*), nuclear (*D*), and cytosolic (*E*) fractions. Data are mean ± SEM. *$P < 0.05$.

The numbers of upregulated and downregulated genes for each nuclei type are presented in Fig. 5*E* and are listed in Supplementary Table 2 and highlight FAPs as the most transcriptionally active, followed by vascular cells and adipocytes (Fig. 5*E*). Enrichment analyses revealed adipocytes had a downregulation of G protein–coupled glutamate receptor signaling pathway, while cytoplasmic translation was upregulated across multiple nuclei types (Fig. 5*F* and Supplementary Table 2). We detected secreted factors identified by the human protein atlas (2,502 total) that were related to cytokines and identified which of those genes were differentially expressed pre- and postintervention for each cell type (228 total) (Fig. 5*G*). The majority of cytokines decreased after the intervention in each cell type, which would be consistent with a less inflammatory IMAT secretome after the intervention.

Skeletal Muscle Bulk RNA-seq

The differential expressions of 605 genes were observed to change significantly over the course of the intervention and were related to insulin sensitivity ($P < 0.05$) (Fig. 6*A*). Genes were further compared with their correlation with changes with relevant outcomes (glucose infusion rate [GIR], body weight, VO_2peak, or BMI) either before or after intervention, where the largest overlap with post-intervention traits was observed for GIR (Fig. 6*B*). Next, individuals were partitioned into participants with either low or high GIR following the intervention, with a cut point of 5 mg/kg/min. This cut point was chosen because it was the average glucose disposal during an insulin clamp in sedentary obese individuals previously reported by our group (29) (Supplementary Fig. 8). Intervention changes associated with high GIR were observed with core muscle pathways and adaption, and low GIR changes were enriched in diverse metabolic pathways (Fig. 6*C*). There were more genes that were significantly correlated with GIR following intervention (Fig. 6*D*) that were enriched in remodeling and apoptosis (Fig. 6*E*). Genes that correlated with GIR only prior to intervention showed enrichments in TOR signaling (Fig. 6*F*), and genes that persisted in their correlation with GIR both pre- and postintervention showed enrichments in mitochondrial pathways (Fig. 6*G*). Given the large changes of nuclear lipids associated with intervention, the association of the change of specific genes with nuclear lipids during the intervention was evaluated. These changes showed distinct pathways associated with alterations in nuclear lipidomes. For example, nuclear DAG expression was related to many genes enriched with cell stress and fiber organization at baseline (Fig. 6*H*), while a positive correlation with phosphofructokinase enzymes and negative enrichment with vitamin D metabolism was observed after the intervention (Fig. 6*I*).

Protein Expression

Before and after the intervention, muscle biopsies during the hyperinsulinemic-euglycemic clamp revealed significant increases in phosphorylation of AKT^{Ser473}/total AKT and $AS160^{Thr642}$/total AS160, without differences in insulin signaling after the intervention compared with before (Fig. 7*A* and *B*). Phosphorylation of inflammatory marker $ERK1/2^{Thr202/Tyr204}$ decreased significantly after the intervention (Fig. 7*C*), with a trend for a decrease in p38 $MAPK^{Thr180/Tyr182}$ ($P = 0.067$) (Fig. 7*E*), without a significant change in the phosphorylation of inflammatory marker $STAT3^{Tyr705}$ (Fig. 7*D*) in the basal samples.

PKC Activation

PKC membrane-to-cytosol ratios, a surrogate for PKC activation, did not change for PKCδ, PKCε, and PKCθ isoforms (Supplementary Fig. 9).

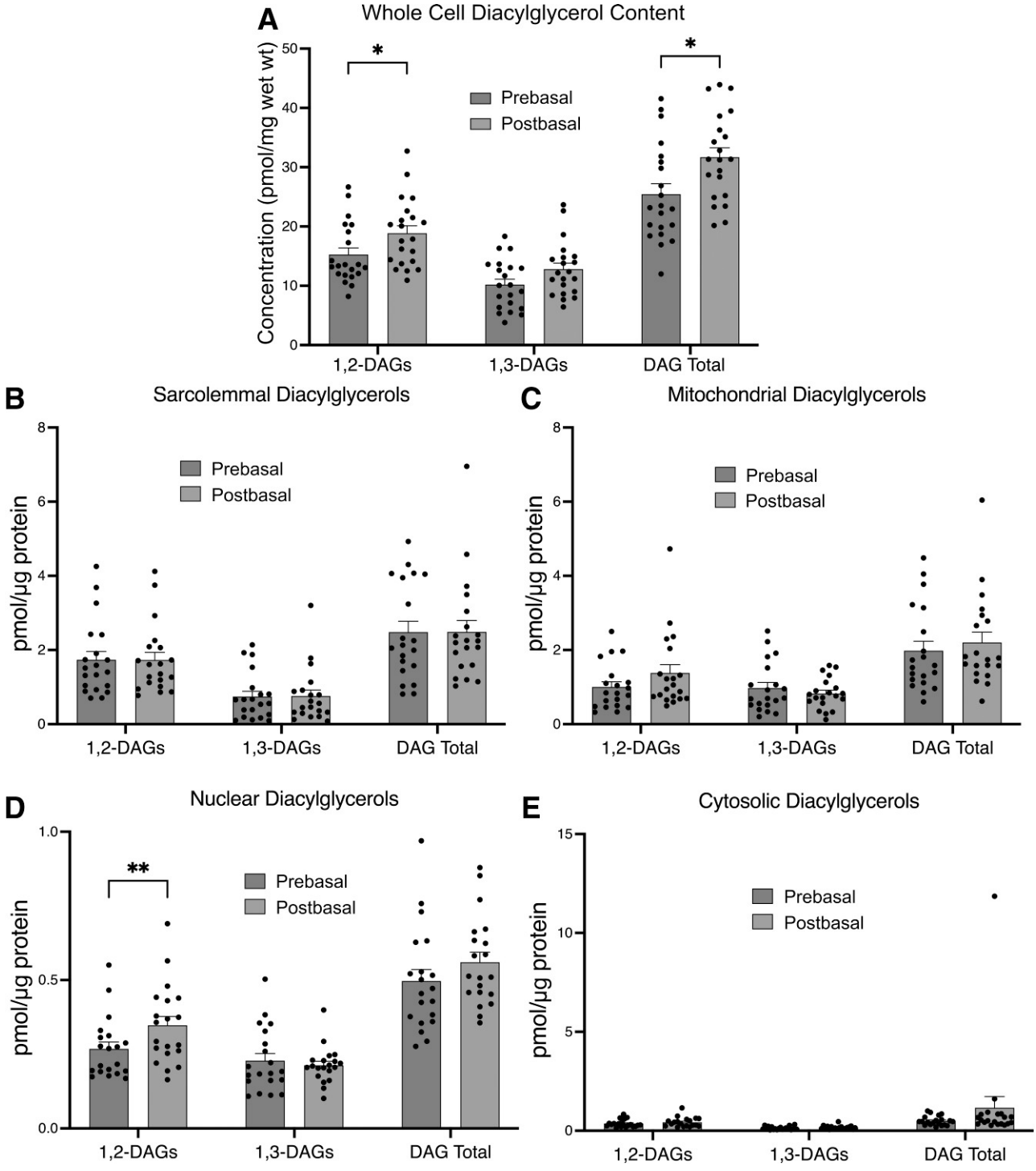

Figure 2—Whole-muscle DAG concentration for 1,2-DAG and 1,3-DAG isomers as well as the sum of all DAG isomers before and after the intervention (*A*). DAG concentrations are shown for sarcolemmal (*B*), mitochondrial (*C*), nuclear (*D*), and cytosolic (*E*) fractions. Data are mean ± SEM. *$P < 0.05$, **$P < 0.01$.

DISCUSSION

Several reports have shown that the localization of bioactive lipids in muscle is related to insulin resistance in rodents and humans (8–10,25,30–32). Importantly, sarcolemmal 1,2-DAG accumulation and sarcolemmal and mitochondrial ceramide accumulation have been associated with lower insulin sensitivity and appear to be important players in cross-sectional comparisons (8,9,30). These cross-sectional comparisons are reinforced by a recent longitudinal study that showed changes in mitochondrial and endoplasmic reticulum ceramide content after weight loss alone (10). Further, administration of IMAT

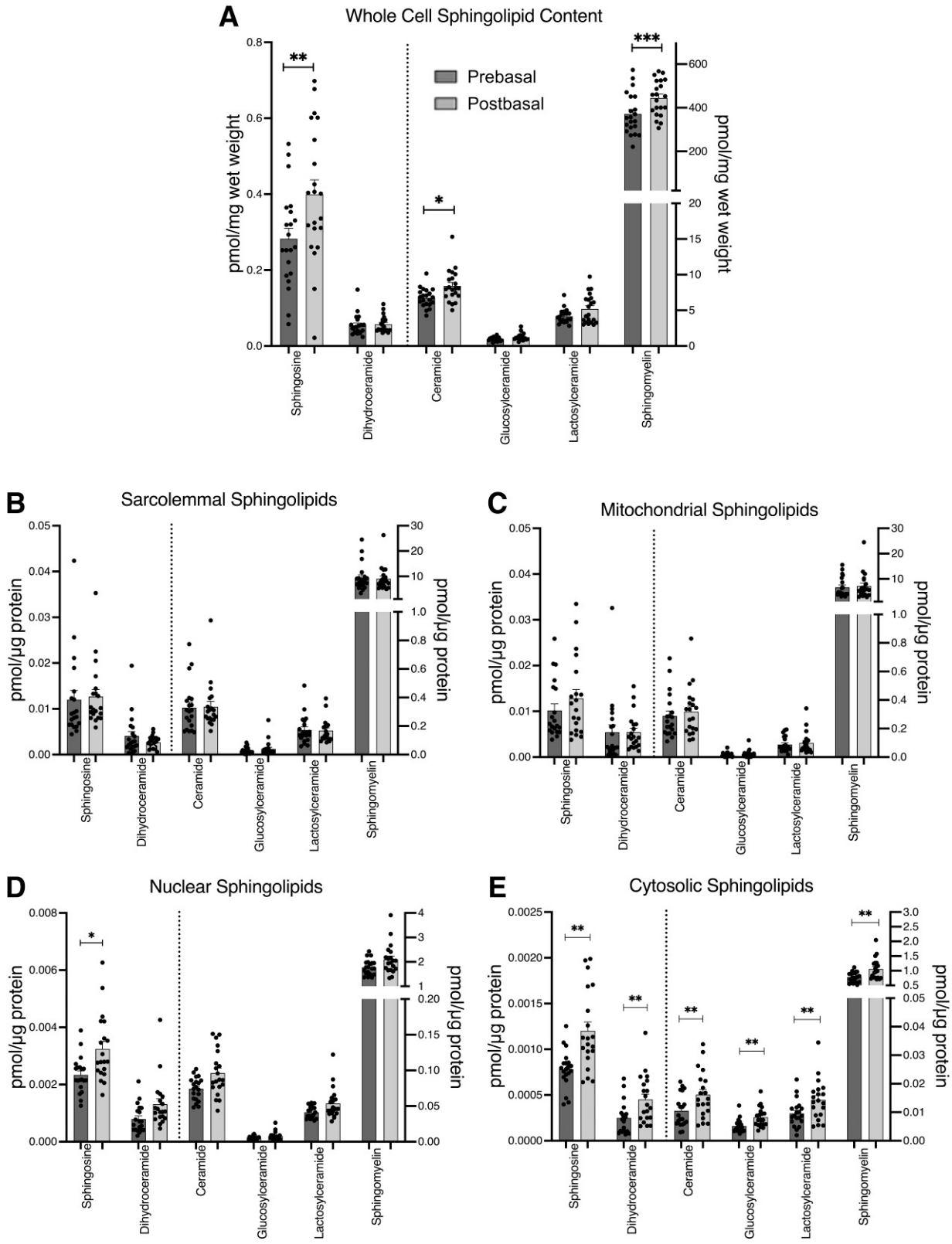

Figure 3—Whole-muscle sphingolipid concentrations for sphingosine, dihydroceramide, ceramide, glucosylceramide, lactosylceramide, and sphingomyelin before and after the intervention (*A*). Sphingolipids concentrations are shown for sarcolemmal (*B*), mitochondrial (*C*), nuclear (*D*), and cytosolic (*E*) fractions. Data are mean ± SEM. **P* < 0.05, ***P* < 0.01, ****P* < 0.001.

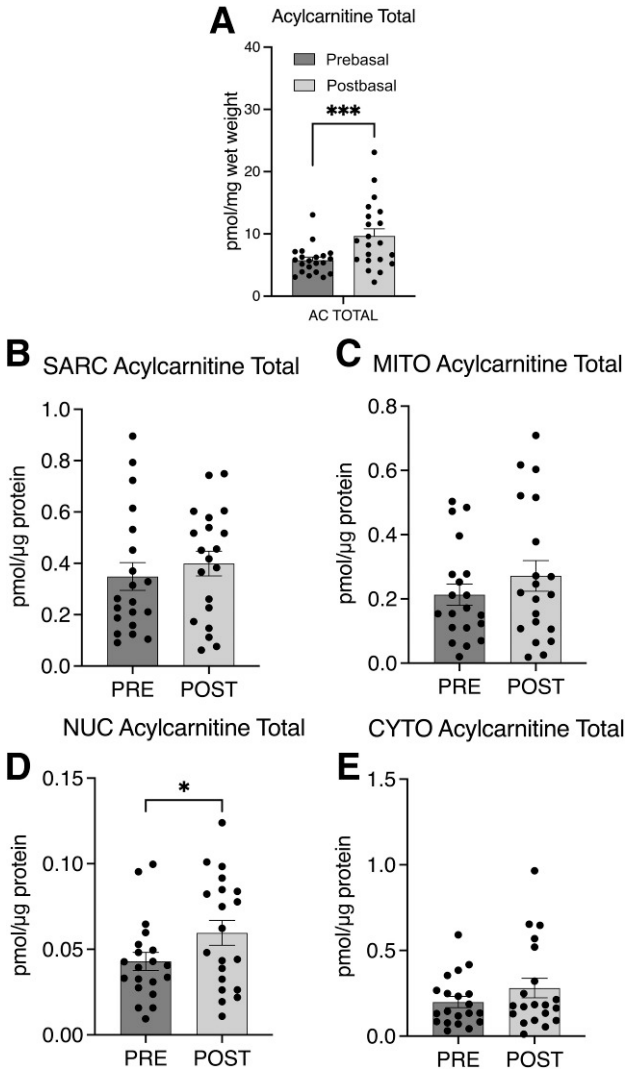

Figure 4—Whole-muscle acylcarnitine concentration before and after the intervention (*A*). Acylcarnitine concentrations are shown for sarcolemmal (*B*), mitochondrial (*C*), nuclear (*D*), and cytosolic (*E*) fractions. Data are mean ± SEM. $*P < 0.05$, $***P < 0.001$.

tissue conditioned media can decrease myotube insulin sensitivity in vitro, with an inflammatory cytokine secretome driven by resident immune cells, the composition of which scales to insulin resistance across a spectrum of metabolic health (14,15). This project was designed to evaluate changes in bioactive lipid localization and IMAT cellular composition after combined weight loss and exercise training intervention in individuals with class I and II obesity. Contrary to our hypothesis, we did not find significant changes in sarcolemmal or mitochondrial content of 1,2-DAG or sphingolipids after the intervention, despite a significant increase in insulin sensitivity, yet we did find changes in IMAT composition of FAP, vascular cells, and immune cells, and the composition of preadipocyte populations. Combined, these data suggest that changes in sarcolemmal and mitochondrial 1,2-DAG and ceramide are not required for muscle insulin sensitization in people with obesity but that changes in IMAT composition and transcriptional profiles occur concomitantly with increased muscle insulin sensitivity after an intensive lifestyle intervention.

Most insulin signaling is thought to occur in the plasma membrane (sarcolemma) of muscle cells. It is therefore likely that sarcolemmal 1,2-DAG and sphingolipids are most closely related to alterations in insulin signaling. This idea is consistent with known mechanisms by which 1,2-DAG and ceramides impact insulin signaling (33–35). Our data are consistent with this idea, as we found no changes in both sarcolemmal lipids and insulin signaling before and after the intervention, and that sphingomyelinase degradation is more important than de novo ceramide synthesis for sarcolemmal ceramide accumulation. Thus, sarcolemmal lipids may negatively impact muscle insulin sensitivity, but decreased sarcolemmal lipids do not appear to be required for insulin sensitization.

Mitochondrial ceramides have been linked to decreased mitochondrial function and insulin resistance in human studies (8,9), and a previous study found mitochondrial ceramides decreased after an insulin-sensitizing weight loss intervention (10). Mitochondria contain sphingomyelinases that produce compartment-specific ceramide in response to inflammation and can inhibit complexes I and III of the electron transport chain (36). This can induce mitochondrial dysfunction and reactive oxygen species production and therefore contribute to insulin resistance (36). These relationships were recently proven experimentally in cell culture with mitochondrial-targeted changes in ceramide content that altered mitochondrial function and insulin sensitivity (30). We did not observe changes in mitochondrial sphingolipids in this study, which was surprising, considering exercise training is known to increase mitochondrial content. These data could be explained by a weight loss–induced decreased inflammation after the intervention, as shown by decreased plasma TNFα concentration and muscle ERK1/2 and p38 MAPK phosphorylation, along with a presumed increase in mitochondrial content after training and associated membrane ceramides that counteracted each other's effects. Previously, we found that mitochondrial/ER 1,2-DAGs were greater in insulin-sensitive athletes and lean individuals, yet we found no differences after the intervention in this study, similar to what was recently reported after weight loss alone (10). After exercise training, our participants were not as insulin-sensitive and active as athletes or lean individuals, which may explain the lack of change. However, it is most likely that combined weight loss and exercise training could confound one another, as weight loss typically reduces many muscle lipids, including TAGs and DAGs, while exercise training consistently increases muscle TAG, with greater DAG reported in endurance-trained athletes (5). Combined, these data suggest that alterations

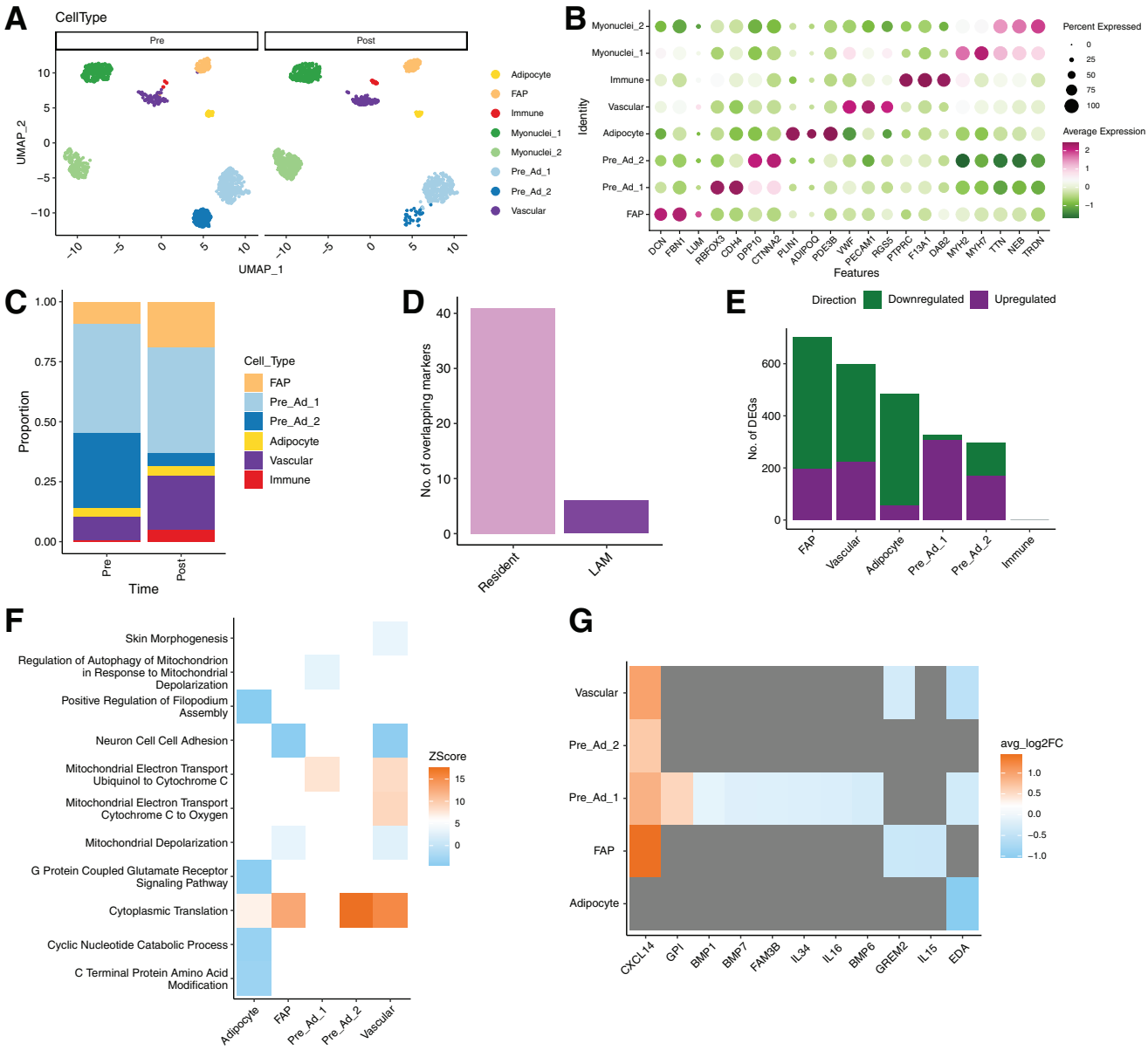

Figure 5— snRNA-seq on pooled IMAT samples before and after the intervention (*A*). Dot plot for the cell types identified (*B*). Proportion of cell types changed after the intervention (*C*), as well as relative gene expression by cell types (*D*). Macrophage gene markers in IMAT (*E*), as well as direction of changes for differentially expressed genes by cell type (*F*). Differentially expressed genes related to cytokines and predicted to be secreted pre- and postintervention (*G*).

in mitochondrial lipids are not required for improved insulin sensitivity.

One of the most unexpected and exciting findings of this study were the changes in nuclear lipids after the combined weight loss and exercise training intervention. There is a considerable amount of lipid in the nucleus of muscle, likely because of the fact that the nuclear membrane is a double lipid bilayer. Additionally, nuclear lipids exist outside the nuclear envelope, as nuclear lipid droplets have been described, nuclear DAG can regulate cell growth, and nuclear sphingolipids can impact chromatin assembly and dynamics (37–39). Very little is known regarding changes in nuclear lipids after insulin-sensitizing interventions. Importantly, nuclear localized 1,2-DAG accumulation was not related to alterations in PKC signaling. One intriguing idea is that alterations in nuclear lipids may alter gene transcription, because specific lipid species such as glycerophospholipids, long chain acyl-CoA, leukotriene B_4, and polyunsaturated fatty acids are known to be nuclear ligands regulating gene transcription (40–43). Further, TAG degradation generated ligands for peroxisome proliferator–activated receptor activation, implicating FFA or DAG as possible lipid ligands (44). We previously reported greater nuclear TAG content in individuals with type 2 diabetes that was inversely related to insulin sensitivity (45), consistent with the current data showing a decrease in nuclear

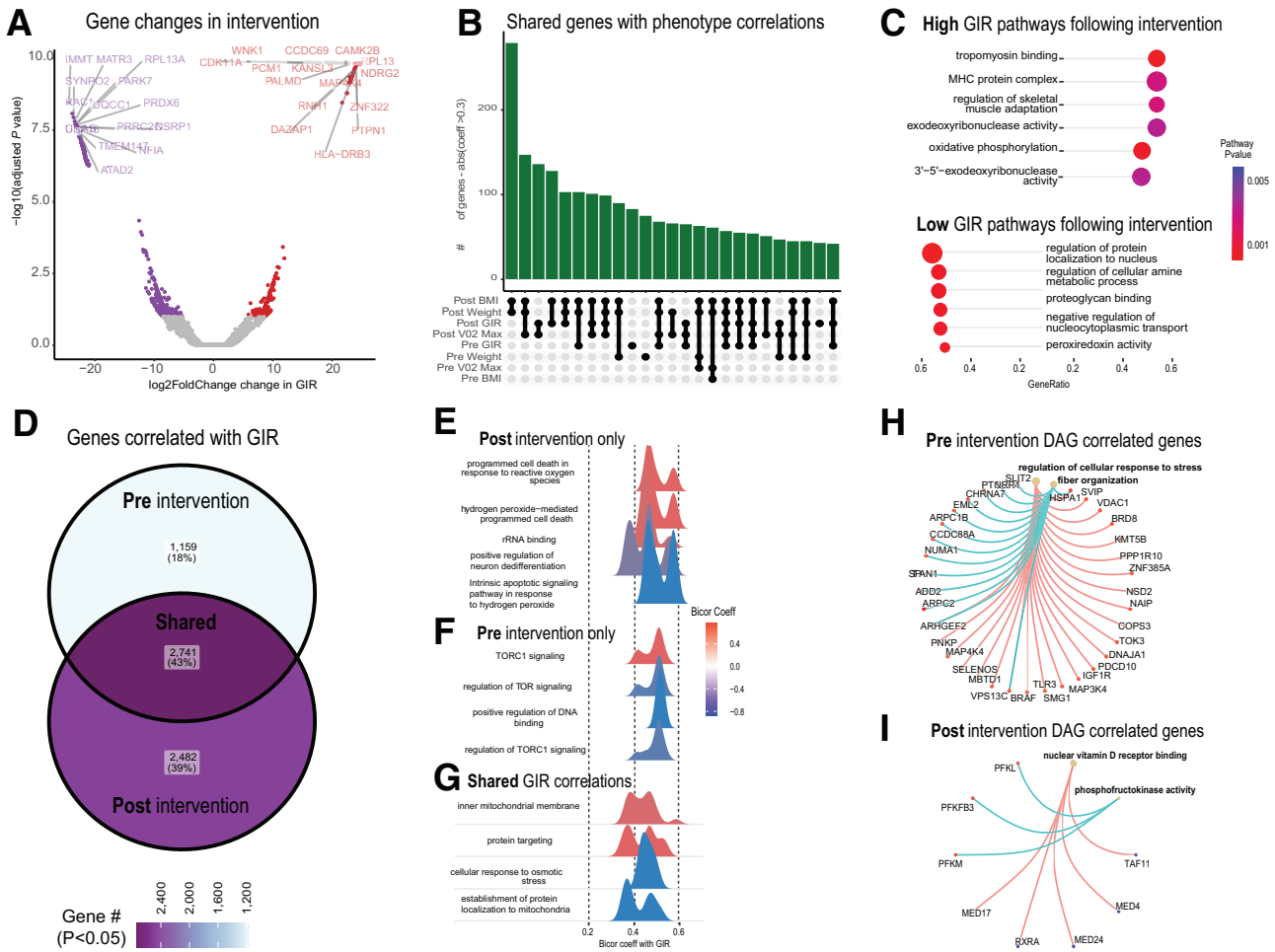

Figure 6—Skeletal muscle RNA-seq analysis before and after the intervention showing significant changes in gene expression (*A*), the number of genes shared with phenotypes (*B*), and pathways associated with high and low GIR following the intervention (*C*). We also evaluated genes (*D*) and pathways (*E–G*) correlated with GIR before and after the intervention. (*H* and *I*) Genes correlated with DAG before and after the intervention.

TAG content after the intervention. Previous data from our laboratory also reported greater nuclear 1,2-DAG in athletes, which is consistent with the current finding of greater nuclear 1,2-DAG after the intervention (8). While speculative, it is possible that changes in nuclear lipid accumulation may impact muscle gene transcription. Consistent with this idea, we found that nuclear 1,2-DAGs were related to cellular response to stress before the intervention, including MAP kinases involved in insulin signaling (MAP4K4, MAP3K4, BRAF), heat shock proteins (HSPA1, DNAJA1), and Toll-like receptor signaling (TLR3), which were not evident after the intervention. Nuclear 1,2-DAGs were related to fewer genes after the intervention, suggesting increased nuclear 1,2-DAGs after combined weight loss and exercise could alter transcription of specific genes specifically related to response to stress.

Inflammation is known to decrease muscle insulin sensitivity, in part by altering insulin signaling and transcription factor activation (46). Following the intervention, we observed reduced phosphorylation of ERK1/2 and a trend for reduced p38 MAPK, which aligns with the decrease in circulating TNFα, a known promoter of both ERK1/2 and p38 MAPK phosphorylation (47). However, despite the decrease in circulating TNFα and inflammatory signaling after the intervention, we did not find changes in insulin signaling. Similar disassociation between insulin sensitivity and signaling has been reported in humans and rodents and could be explained by only a portion of PI3K activation required for full stimulation of AKT, total changes in insulin signaling possibly not reflecting changes in specific submembrane compartments, and alterations in insulin-stimulated translocation of AKT to the sarcolemma (48–51). Insulin resistance can also occur in the microvasculature, resulting in attenuated insulin-induced vasodilation, delivery of insulin and glucose to muscle, and insulin-stimulated muscle glucose uptake independent of changes in myofiber insulin sensitivity (52,53). Our data suggest that changes in chronic activation of ERK1/2 and p38 MAPK signaling, which can decrease GLUT4 and PGC1α expression and contribute to mitochondrial dysfunction and

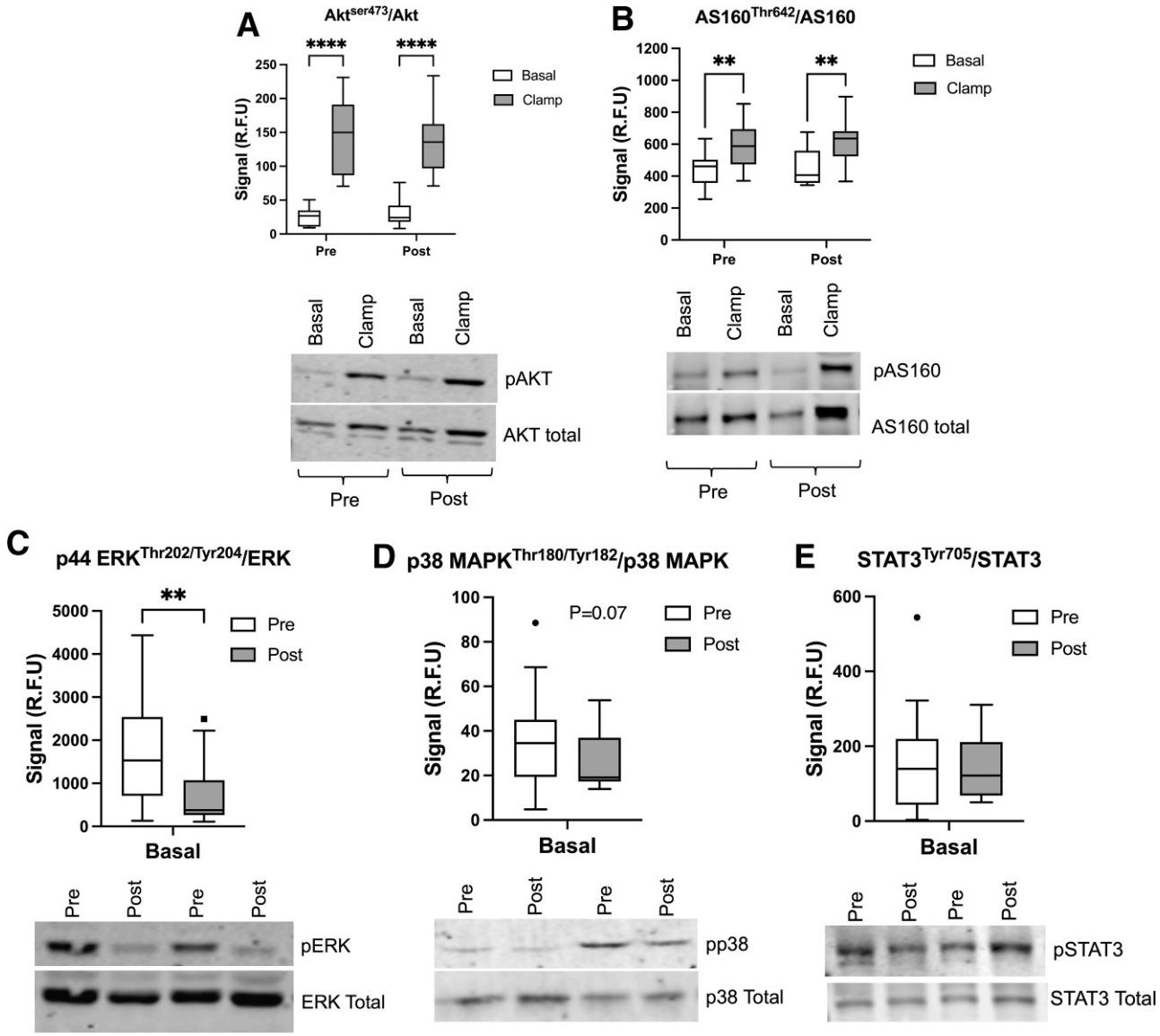

Figure 7—Western analysis of basal and insulin-stimulated skeletal muscle biopsies showing changes in AKT^{ser473}/total (*A*), and AS^{160Thr642}/total (*B*) before and after the intervention. Changes in p44/p42 ERK$^{Thr202/204}$/total (*C*), p38 MAPK$^{Thr180/Tyr182}$/total (*D*), and STAT3^{Tyr705}/total (*E*) in basal biopsies before and after the intervention. Data are mean ± SEM. *$P < 0.05$, **$P < 0.01$, ****$P < 0.0001$. Signal R.F.U., relative fluorescence units.

oxidative stress (54,55), may help explain improvements in insulin sensitivity after the intervention.

Paracrine signaling from IMAT is an important player in muscle insulin sensitivity, as the IMAT secretome is more inflammatory than visceral adipose tissue (15) and can decrease muscle insulin sensitivity in vitro (14). The cellular composition of adipose tissue dictates its secretome, and IMAT is composed of multiple cell types, including immune cells and preadipocytes, which explains its inflammatory signature and metabolic potency (15,16). Preadipocytes are known to secrete extracellular matrix proteins, growth factors, and angiogenesis inhibitors (56) and correlate strongly with metabolic disease (57). The Pre_Ad_2 population that was characterized by γ-aminobutyric acid signaling gene signatures decreased after the intervention, which may help explain the increase in insulin sensitivity. Decreased preadipocytes may reduce the pool of adipocyte progenitors from which adipocytes form in favor of a less committed progenitor cell (FAPs) and partially explain reduced IMAT content with weight loss (58), or the ability of exercise to prevent IMAT accumulation (59). Intriguingly, γ-butyric acid signaling has been linked to decreased macrophage infiltration in subcutaneous but not visceral adipose tissue in mice (60). In agreement with a reduced Pre_Ad_2 γ-butyric acid signaling and previous reports from our laboratory (28), we observed an increase in macrophage proportions after the intervention that had a more anti-inflammatory "M2"

resident phenotype, which is associated with decreased inflammation, lipid buffering, and regulation of immune cells and thus represents healthy IMAT remodeling (28). Increased vascular cells in IMAT after the intervention may reflect an increase in capillarization and overall adipose tissue remodeling, which has been shown in subcutaneous adipose tissue after exercise training interventions (61), and may reduce adipose tissue hypoxia that can lead to fibrosis, inflammation, and insulin resistance (62). Differentially expressed genes within each of the IMAT cell types also revealed decreased expression of secreted cytokines and inflammatory proteins, consistent with a less inflammatory IMAT secretome with a less negative impact on muscle insulin sensitivity. Combined, significant changes in the IMAT cell composition may help explain the increase in insulin sensitivity following the combined weight loss and exercise training intervention.

There are several limitations to this work that are important to recognize. We did not include a control weight stable, weight loss–only, or exercise training–only group in this study, which may have masked some lipid alterations following this intervention and prevents distinguishing intervention effects from effects of time or biopsy sampling. Participants had obesity and insulin resistance prior to entering the study; therefore, we do not know whether the intervention returned these individuals to a more insulin-sensitive state similar to a never-obese condition or whether our results reflect that the muscle first adapted to the obese condition before the insulin-sensitizing intervention. It is possible that it takes longer than 12 weeks and more substantial weight loss to see changes in sarcolemmal and mitochondrial DAG and ceramide content. Additionally, we controlled diet for 7 days prior to the muscle biopsy and insulin clamp days, and it is possible that this controlled diet altered muscle lipid species relative to their normal diet, which could have changed localized lipids. Our intervention was performed predominantly in women, and therefore our results may not be translatable to men. The age range of our participants likely included both pre- and postmenopausal women, which could have added variability to our results. We do not know the functional significance of changes in IMAT cellular composition, and so we are speculating on the physiological relevance of these changes on the IMAT secretome. The IMAT snRNA-seq was performed on pooled samples that did not permit subject-level analyses. Finally, it is likely that there are submembrane regions of the sarcolemma that may have localized differences in lipids, such as in caveoli or t-tubules, that are not captured and would be missed by this method.

These data indicate that changes in sarcolemmal ceramide and DAG are not required for insulin sensitization after a combined weight loss and exercise training intervention in people with obesity, prediabetes, and type 2 diabetes. However, this intervention dramatically changed IMAT cellular composition, and therefore the IMAT secretome, which is known to decrease muscle insulin sensitivity.

Funding. This work was supported by National Institutes of Health General Clinical Research Center grant RR-00036, an American Diabetes Association grant to B.C.B. (1-14-CE-05), and Colorado Nutrition Obesity Research Center grant P30DK048520.

Duality of Interest. No potential conflicts of interest relevant to this article were reported.

Author Contributions. K.Z.B. performed lipidomic analysis of whole muscle and subcellular fractions and helped with data interpretation and manuscript preparation. A.G. developed the subcellular fractionation protocol, isolated subcellular fractions from all the biopsies, helped with subject testing, and edited the manuscript. E.M. performed muscle membrane and cytosolic isolations and Western analysis for PKC activation and edited the manuscript. S.Z. helped with subject recruitment and testing, whole muscle lipidomic analysis, data interpretation, and manuscript preparation. P.J. and T.S. performed antibody optimization and the Western analysis of muscle biopsies and helped edit the manuscript. S.B. derivatized plasma samples for glucose kinetics analysis. L.P. helped design the study, provided medical oversight, performed all biopsies, and helped write the manuscript. C.J. ran the glucose kinetics by gas chromatography–mass spectrometry. D.K. helped with subject recruitment and testing, data interpretation, and manuscript preparation. A.K. helped with subject recruitment and testing, data interpretation, and manuscript preparation. K.L.W., Y.S., M.W., and L.M.S. performed the snRNA-seq analysis and helped write and edit the manuscript. I.J.T., C.M.N., C.H.V., and M.S. performed the RNA-seq analysis and interpretation of muscle biopsies from this study and helped edit the manuscript. B.C.B. designed the study, performed subject testing, dissected all muscle biopsies, analyzed data, and wrote the manuscript. B.C.B. is the guarantor of this work and, as such, had full access to all the data in the study and takes responsibility for the integrity of the data and the accuracy of the data analysis.

Prior Presentation. Parts of this study were presented in abstract form at the Lipidomics Gordon Research Conference, Barga, Italy, 5–10 May 2024.

References

1. Goodpaster BH, He J, Watkins S, Kelley DE. Skeletal muscle lipid content and insulin resistance: evidence for a paradox in endurance-trained athletes. J Clin Endocrinol Metab 2001;86:5755–5761

2. Bergman BC, Brozinick JT, Strauss A, et al. Muscle sphingolipids during rest and exercise: a C18:0 signature for insulin resistance in humans. Diabetologia 2016;59:785–798

3. Turpin SM, Nicholls HT, Willmes DM, et al. Obesity-induced CerS6-dependent C16:0 ceramide production promotes weight gain and glucose intolerance. Cell Metab 2014;20:678–686

4. Turpin-Nolan SM, Hammerschmidt P, Chen W, et al. CerS1-derived C18:0 ceramide in skeletal muscle promotes obesity-induced insulin resistance. Cell Rep 2019;26:1–10.e7.e17

5. Amati F, Dubé JJ, Alvarez-Carnero E, et al. Skeletal muscle triglycerides, diacylglycerols, and ceramides in insulin resistance: another paradox in endurance-trained athletes? Diabetes 2011;60:2588–2597

6. Coen PM, Dubé JJ, Amati F, et al. Insulin resistance is associated with higher intramyocellular triglycerides in type I but not type II myocytes concomitant with higher ceramide content. Diabetes 2010;59:80–88

7. Dubé JJ, Amati F, Toledo FGS, et al. Effects of weight loss and exercise on insulin resistance, and intramyocellular triacylglycerol, diacylglycerol and ceramide. Diabetologia 2011;54:1147–1156

8. Perreault L, Newsom SA, Strauss A, et al. Intracellular localization of diacylglycerols and sphingolipids influences insulin sensitivity and mitochondrial function in human skeletal muscle. JCI Insight 2018;3:e96805

9. Chung JO, Koutsari C, Blachnio-Zabielska AU, Hames KC, Jensen MD. Intramyocellular ceramides: subcellular concentrations and fractional de novo synthesis in postabsorptive humans. Diabetes 2017;66:2082–2091
10. Petersen MC, Yoshino M, Smith GI, et al. Effect of weight loss on skeletal muscle bioactive lipids in people with obesity and type 2 diabetes. Diabetes 2024;73:2055–2064
11. Boettcher M, Machann J, Stefan N, et al. Intermuscular adipose tissue (IMAT): association with other adipose tissue compartments and insulin sensitivity. J Magn Reson Imaging 2009;29:1340–1345
12. Song M-Y, Ruts E, Kim J, Janumala I, Heymsfield S, Gallagher D. Sarcopenia and increased adipose tissue infiltration of muscle in elderly African American women. Am J Clin Nutr 2004;79:874–880
13. Gallagher D, Kuznia P, Heshka S, et al. Adipose tissue in muscle: a novel depot similar in size to visceral adipose tissue. Am J Clin Nutr 2005;81: 903–910
14. Sachs S, Zarini S, Kahn DE, et al. Intermuscular adipose tissue directly modulates skeletal muscle insulin sensitivity in humans. Am J Physiol Endocrinol Metab 2019;316:E866–E879
15. Kahn D, Macias E, Zarini S, et al. Quantifying the inflammatory secretome of human intermuscular adipose tissue. Physiol Rep 2022;10:e15424
16. Elingaard-Larsen LO, Whytock KL, Divoux A, et al. Isolation of nuclei from human intermuscular adipose tissue and downstream single-nuclei RNA sequencing. J Vis Exp 2024:10.3791/66784
17. Grunwald GK, Melanson EL, Forster JE, Seagle HM, Sharp TA, Hill JO. Comparison of methods for achieving 24-hour energy balance in a whole-room indirect calorimeter. Obes Res 2003;11:752–759
18. Guo Z, Mishra P, Macura S. Sampling the intramyocellular triglycerides from skeletal muscle. J Lipid Res 2001;42:1041–1048
19. Bijker KE, de Groot G, Hollander AP. Differences in leg muscle activity during running and cycling in humans. Eur J Appl Physiol 2002;87:556–561
20. Harrison KA, Bergman BC. HPLC-MS/MS methods for diacylglycerol and sphingolipid molecular species in skeletal muscle. Methods Mol Biol 2019; 1978:137–152
21. Whytock KL, Divoux A, Sun Y, et al. Isolation of nuclei from frozen human subcutaneous adipose tissue for full-length single-nuclei transcriptional profiling. STAR Protoc 2023;4:102054
22. Whytock KL, Divoux A, Sun Y, et al. Aging human abdominal subcutaneous white adipose tissue at single cell resolution. Aging Cell 2024;23:e14287
23. Yang S, Corbett SE, Koga Y, et al. Decontamination of ambient RNA in single-cell RNA-seq with DecontX. Genome Biol 2020;21:57
24. Korsunsky I, Millard N, Fan J, et al. Fast, sensitive and accurate integration of single-cell data with Harmony. Nat Methods 2019;16:1289–1296
25. Bergman BC, Hunerdosse DM, Kerege A, Playdon MC, Perreault L. Localisation and composition of skeletal muscle diacylglycerol predicts insulin resistance in humans. Diabetologia 2012;55:1140–1150
26. Bergman BC, Howard D, Schauer IE, et al. Features of hepatic and skeletal muscle insulin resistance unique to type 1 diabetes. J Clin Endocrinol Metab 2012;97:1663–1672
27. Dobrzyn A, Gorski J. Ceramides and sphingomyelins in skeletal muscles of the rat: content and composition. Effect of prolonged exercise. Am J Physiol Endocrinol Metab 2002;282:E277–E285
28. Ahn C, Divoux A, Zhou M, Seldin MM, Sparks LM, Whytock KL. Optimized RNA sequencing deconvolution illustrates the impact of obesity and weight loss on cell composition of human adipose tissue. Obesity (Silver Spring) 2025;33:936–948
29. Zarini S, Brozinick JT, Zemski Berry KA, et al. Serum dihydroceramides correlate with insulin sensitivity in humans and decrease insulin sensitivity in vitro. J Lipid Res 2022;63:100270
30. Diaz-Vegas A, Madsen S, Cooke KC, et al. Mitochondrial electron transport chain, ceramide, and coenzyme Q are linked in a pathway that drives insulin resistance in skeletal muscle. Elife 2023;12:RP87340
31. Nowotny B, Zahiragic L, Krog D, et al. Mechanisms underlying the onset of oral lipid-induced skeletal muscle insulin resistance in humans. Diabetes 2013;62:2240–2248
32. Lee H-Y, Choi CS, Birkenfeld AL, et al. Targeted expression of catalase to mitochondria prevents age-associated reductions in mitochondrial function and insulin resistance. Cell Metab 2010;12:668–674
33. Itani SI, Zhou Q, Pories WJ, MacDonald KG, Dohm GL. Involvement of protein kinase C in human skeletal muscle insulin resistance and obesity. Diabetes 2000;49:1353–1358
34. Dobrowsky RT, Kamibayashi C, Mumby MC, Hannun YA. Ceramide activates heterotrimeric protein phosphatase 2A. J Biol Chem 1993;268:15523–15530
35. Powell DJ, Hajduch E, Kular G, Hundal HS. Ceramide disables 3-phosphoinositide binding to the pleckstrin homology domain of protein kinase B (PKB)/Akt by a PKCzeta-dependent mechanism. Mol Cell Biol 2003;23:7794–7808
36. García-Ruiz C, Colell A, Marí M, Morales A, Fernández-Checa JC. Direct effect of ceramide on the mitochondrial electron transport chain leads to generation of reactive oxygen species. Role of mitochondrial glutathione. J Biol Chem 1997;272:11369–11377
37. Topham MK, Bunting M, Zimmerman GA, McIntyre TM, Blackshear PJ, Prescott SM. Protein kinase C regulates the nuclear localization of diacylglycerol kinase-zeta. Nature 1998;394:697–700
38. Lucki NC, Sewer MB. Nuclear sphingolipid metabolism. Annu Rev Physiol 2012;74:131–151
39. Ohsaki Y, Kawai T, Yoshikawa Y, Cheng J, Jokitalo E, Fujimoto T. PML isoform II plays a critical role in nuclear lipid droplet formation. J Cell Biol 2016;212:29–38
40. Hertz R, Magenheim J, Berman I, Bar-Tana J. Fatty acyl-CoA thioesters are ligands of hepatic nuclear factor-4α. Nature 1998;392:512–516
41. Devchand PR, Keller H, Peters JM, Vazquez M, Gonzalez FJ, Wahli W. The PPARα-leukotriene B4 pathway to inflammation control. Nature 1996;384:39–43
42. Krylova IN, Sablin EP, Moore J, et al. Structural analyses reveal phosphatidyl inositols as ligands for the NR5 orphan receptors SF-1 and LRH-1. Cell 2005;120:343–355
43. Zechner R, Zimmermann R, Eichmann TO, et al. FAT SIGNALS–lipases and lipolysis in lipid metabolism and signaling. Cell Metab 2012;15:279–291
44. Haemmerle G, Moustafa T, Woelkart G, et al. ATGL-mediated fat catabolism regulates cardiac mitochondrial function via PPAR-α and PGC-1. Nat Med 2011;17:1076–1085
45. Kahn D, Perreault L, Macias E, et al. Subcellular localisation and composition of intramuscular triacylglycerol influence insulin sensitivity in humans. Diabetologia 2021;64:168–180
46. Shoelson SE, Lee J, Goldfine AB. Inflammation and insulin resistance. J Clin Invest 2006;116:1793–1801
47. Li Y-P, Chen Y, John J, et al. TNF-α acts via p38 MAPK to stimulate expression of the ubiquitin ligase atrogin1/MAFbx in skeletal muscle. Faseb J 2005;19:362–370
48. Kruszynska YT, Worrall DS, Ofrecio J, Frias JP, Macaraeg G, Olefsky JM. Fatty acid-induced insulin resistance: decreased muscle PI3K activation but unchanged Akt phosphorylation. J Clin Endocrinol Metab 2002;87:226–234
49. Kim YB, Nikoulina SE, Ciaraldi TP, Henry RR, Kahn BB. Normal insulin-dependent activation of Akt/protein kinase B, with diminished activation of phosphoinositide 3-kinase, in muscle in type 2 diabetes. J Clin Invest 1999;104:733–741
50. Kim YB, Zhu JS, Zierath JR, Shen HQ, Baron AD, Kahn BB. Glucosamine infusion in rats rapidly impairs insulin stimulation of phosphoinositide 3-kinase but does not alter activation of Akt/protein kinase B in skeletal muscle. Diabetes 1999;48:310–320
51. Fasshauer M, Klein J, Ueki K, et al. Essential role of insulin receptor substrate-2 in insulin stimulation of Glut4 translocation and glucose uptake in brown adipocytes. J Biol Chem 2000;275:25494–25501
52. Broussard JL, Castro AVB, Iyer M, et al. Insulin access to skeletal muscle is impaired during the early stages of diet-induced obesity. Obesity (Silver Spring) 2016;24:1922–1928

53. Parry SA, Turner MC, Woods RM, et al. High-fat overfeeding impairs peripheral glucose metabolism and muscle microvascular eNOS Ser1177 phosphorylation. J Clin Endocrinol Metab 2020;105:dgz018
54. Ho RC, Alcazar O, Fujii N, Hirshman MF, Goodyear LJ. p38γ MAPK regulation of glucose transporter expression and glucose uptake in L6 myotubes and mouse skeletal muscle. Am J Physiol Regul Integr Comp Physiol 2004;286:R342–R349
55. Hwang S-L, Jeong Y-T, Li X, et al. Inhibitory cross-talk between the AMPK and ERK pathways mediates endoplasmic reticulum stress-induced insulin resistance in skeletal muscle. Br J Pharmacol 2013;169:69–81
56. Hocking SL, Wu LE, Guilhaus M, Chisholm DJ, James DE. Intrinsic depot-specific differences in the secretome of adipose tissue, preadipocytes, and adipose tissue-derived microvascular endothelial cells. Diabetes 2010;59: 3008–3016
57. Reinisch I, Ghosh A, Noé F, et al. Unveiling adipose populations linked to metabolic health in obesity. Cell Metab 2025;37:640–655.e4
58. Goss AM, Gower B, Soleymani T, et al. Effects of weight loss during a very low carbohydrate diet on specific adipose tissue depots and insulin sensitivity in older adults with obesity: a randomized clinical trial. Nutr Metab (Lond) 2020;17:64
59. Goodpaster BH, Chomentowski P, Ward BK, et al. Effects of physical activity on strength and skeletal muscle fat infiltration in older adults: a randomized controlled trial. J Appl Physiol (1985) 2008;105:1498–1503
60. Hwang I, Jo K, Shin KC, et al. GABA-stimulated adipose-derived stem cells suppress subcutaneous adipose inflammation in obesity. Proc Natl Acad Sci U S A 2019;116:11936–11945
61. Ahn C, Ryan BJ, Schleh MW, et al. Exercise training remodels subcutaneous adipose tissue in adults with obesity even without weight loss. J Physiol 2022;600:2127–2146
62. Halberg N, Khan T, Trujillo ME, et al. Hypoxia-inducible factor 1α induces fibrosis and insulin resistance in white adipose tissue. Mol Cell Biol 2009; 29:4467–4483